Two Conformational States of Turkey Ovomucoid Third Domain at Low pH: Three-Dimensional Structures, Internal Dynamics, and Interconversion Kinetics and Thermodynamics †, ‡

ARTICLE *in* BIOCHEMISTRY · JUNE 2003

Impact Factor: 3.02 · DOI: 10.1021/bi034053f · Source: PubMed

Two Conformational States of Turkey Ovomucoid Third Domain at Low pH: Three-Dimensional Structures, Internal Dynamics, and Interconversion Kinetics and Thermodynamics[†,‡]

Jikui Song,[§] Michael Laskowski, Jr.,[||] M. A. Qasim,[||] and John L. Markley*[,§]

National Magnetic Resonance Facility, Department of Biochemistry, University of Wisconsin−Madison, 433 Babcock Drive, Madison, Wisconsin 53706, and Department of Chemistry, Purdue University, West Lafayette, Indiana 47907

Received January 13, 2003; Revised Manuscript Received March 21, 2003

ABSTRACT: Turkey ovomucoid third domain (OMTKY3) is shown to exist at low pH as two distinctly folded, interconverting conformations. Activation parameters were determined for the transition, and these were of the type reported previously for cis/trans isomerizations of prolyl peptide bonds. Multidimensional, multinuclear NMR spectroscopy was used to determine the three-dimensional structure of each of the two states of P_5-Pro^{14}Asp OMTKY3 at pH 2.5 and 25 °C, under conditions where the two states have equal populations with interchange rates of 0.25 s^{-1}. The results showed that the two states differ by cis/trans isomerization of the P_8-Tyr^{11}−P_7-Pro^{12} peptide bond, which is cis in the conformer dominant at neutral pH and trans in the conformer appearing at low pH. The major structural differences were found to be in the region of the reactive site loop. The core of the protein, including the antiparallel β-sheet and a α-helix, is preserved in both structures. The state with the cis peptide bond is similar to previously reported structures of OMTKY3 determined by NMR spectroscopy and X-ray crystallography. The cis-to-trans transition results in the relocation of the aromatic ring of P_8-Tyr^{11}, disrupts many interactions between the α-helix and the reactive-site loop, and leads to more open spacing between this loop and the α-helix. In addition, the configurations of two of the three disulfide bonds, P_{11}−Cys^8− P_{20}'−Cys^{38}, and P_3−Cys^{16}− P_{17}'−Cys^{35}, are altered such that the C^α−C^α distances for each disulfide bridge are longer by ∼1 Å in the trans state than in the cis. Mutations at P_1-Leu^{18}, P_6-Lys^{13}, and P_5-Pro^{14} influence the position of the cis ⇄ trans equilibrium. In P_1-Leu^{18}Xxx OMTKY3 mutants, the trans state is more favored by P_1-Gly^{18} than by Ala^{18} or Leu^{18}; in P_6-Lys^{13}Xxx OMTKY3 mutants, the trans state is more favored by P_6-Glu^{13} and P_6-Asp^{13} than Lys^{13} or His^{13}. Stabilization of the trans state in P_5-Pro^{14}Xxx OMTKY3 mutants follows the series Xxx = Gly > Asp > Glu > Ala ∼ His > Pro. In comparing the state with the trans peptide bond to that with the cis, the pK_a values of P_{12}-Asp^7 and P_1'-Glu^{19} are higher and those of P_9-Glu^{10} and P_{25}'-Glu^{43} are lower. The pK_a values of other titrating groups in the molecule are similar in both conformational states. These pK_a changes underlie the pH dependence of the conformational equilibrium and can be explained in part by observed structural differences. ^{15}N transverse relaxation results indicate that residues P_6-Lys^{13}-P_3−Cys^{16} in the trans state undergo a dynamic process on the microsecond−millisecond time scale not present in the cis state.

Turkey ovomucoid third domain, OMTKY3 (Figure 1), and bovine pancreatic trypsin inhibitor, BPTI, are the two most- and best-studied, small molecular weight, standard-mechanism (*2*), canonical (*3*) protein inhibitors of serine proteinases. OMTKY3 was first isolated as a 56-amino acid limited-proteolysis fragment from whole ovomucoid, the second most abundant (after ovalbumin) protein from egg white (*4*). The protein is monomeric and stable over a broad pH range (pH 1−12) (*5*). Two types of conformational heterogeneity have been observed in OMTKY3 at low pH. The first is the low pH transition (pH_{mid} 2.8) observed initially by optical spectroscopy in whole chicken ovomucoid (*6*); this "Donovan transition" has been assumed to be triggered by deprotonation of an acidic group in the protein.

[†] This work was supported by NIH Grants RR 02301 (to J.L.M.) and GM 10831 and GM 63539 (to M.L.).

[‡] Structures have been deposited at the Protein Data Bank (trans state at pH 2.5, PDB code 1M8C; cis state at pH 2.5, PDB code 1M8B) and NMR data at the BioMagResBank (trans state at pH 2.5, bmr 5473; cis state at pH 2.5, bmr 5472).

* To whom correspondence should be addressed. Phone: +1 (608) 263-9349. Fax: +1 (608) 262-3759. E-mail: markley@nmrfam.wisc.edu.

[§] University of Wisconsin−Madison.

[||] Purdue University.

[1] Nomenclature: OMTKY3 stands for the third domain of the proteinase inhibitor (ovomucoid) from turkey (*Meleagris gallopavo*), Swiss-Prot P01004. Residues in OMTKY3 are denoted as P_i -Xxx^j, where P denotes the Schecter−Berger notation for proteinase inhibitors (*1*) with *i* values for residues to the N-terminal side of the cleavage site and *i*′ values for those to the C-terminal side, Xxx is the three-letter amino acid code, and *j* is the residue number according to 56-residue OMTKY3 domain (starting with the sequence L^1AAVS^5...). OMTKY3 mutants are also described by dual notation, e.g., P_5-Pro^{14}Asp for substitution of P_5-Pro^{14} by Asp. *C* denotes the state of OMTKY3 with the cis P_8-Tyr^{11}−P_7-Pro^{12} peptide bond, and *T* denotes the state with the trans peptide bond. Abbreviations: DTT, dithiothreitol; DSS, 4,4-dimethyl-4-silapentane-1-sulfonate; *E. coli*, *Escherichia coli*; GdmCl, guanidinium chloride; OMTKY3(6−56), OMTKY3 consisting of residues 6−56; rmsd, root-mean-squared deviation; SNase, staphylococcal nuclease; TPPI, time-proportional phase incrementation.

10.1021/bi034053f CCC: $25.00
Published on Web 05/08/2003

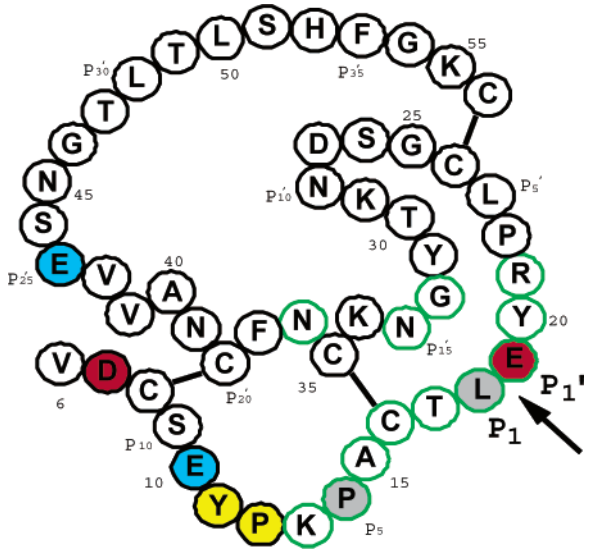

FIGURE 1: Primary structure of turkey ovomucoid third domain, OMTKY3. Residues in the consensus region of contact with serine proteinases are outlined in green. The arrow indicates the reactive-site peptide bond. The conformational transition studied here is linked to cis/trans isomerism about the peptide bond joining residues P_8-Tyr[11] and P_7-Pro[12] (highlighted in yellow). This bond normally is cis, but when P_5-Pro[14] is mutated to other residues or when P_1-Leu[18] is mutated to Gly or His, the trans configuration becomes more highly populated. Residues colored red and blue are ones whose pK_a is shifted up or down, respectively, as the result of the cis → trans transition. The conformational heterogeneity is abolished by mutation of P_7-Pro[12] to Gly.

The second is a transition observable by NMR spectroscopy at low pH, which leads to doubling of peaks (*7*). Because this transition affects the local environment of residues in the consensus contact region with serine proteinases (residues outlined in green in Figure 1), the structural consequences of this transition and its dependence on the identity of residues in the contact region are of considerable interest. We report here that the transition involves cis ⇄ trans isomerization of the P_8-Tyr[11]− P_7-P_{ro}[12] peptide bond, rearrangement of two of the three disulfide bridges in the molecule, and enhanced internal dynamics of residues P_6-Lys[13]−P_3-Cys[16]. We use the notation *C* for the state shown to contain the cis P_8-Tyr[11]−P_7-Pro[12] peptide bond and *T* for the state shown to contain the trans peptide bond. Mutations of residues in the region of OMTKY3 that contacts serine proteinases were found to affect the equilibrium between *C* and *T*. Three-dimensional structures of the individual *C* and *T* states have been determined under conditions where they are equally populated. The dependence of the equilibrium on pH can be explained by structural differences that change pK_a values of individual residues. These results complement the large database of sequence structure−function relationships in avian ovomucoid third domains (*8*).

EXPERIMENTAL PROCEDURES

Protein Expression and Purification. Variants of OMTKY3(6−56) with P_5 residue substitutions (Ala, Asp, Gly, Glu, and His) were prepared at Purdue University according to published procedures (*9*). OMTKY3 variants produced at Wisconsin, which consisted of residues 1−56, were produced as described elsewhere (*10*, *11*).

NMR Sample Preparation. Samples used for NMR pH titration studies were prepared by dissolving protein previously lyophilized from water in one of the two solvents described below to give a final protein concentration of approximately 2−3 mM. The two solvents, which differed only in the content of D_2O (90% H_2O/10% D_2O or 100% D_2O); each contained 100 mM potassium chloride, 0.02% sodium azide, 2% (v/v) of a proteinase inhibitor cocktail (Product no. P 2714, Sigma Chemical Co., Saint Louis, MO, dissolved in 1 mL), and 1 mM DSS as an internal chemical shift reference. The pH of the sample was measured at room temperature, both before and after the NMR data were collected; if these measurements differed by more than 0.10 pH unit, the spectrum was not used. The glass electrode (Biological Combination Electrode, Beckman, Fullerton, CA) was calibrated with commercial standard buffers at pH 1.0, 4.0, and 7.0 (Fisher Scientific, Fair Lawn, NJ).

NMR Spectroscopy. NMR data were collected at the National Magnetic Resonance Facility at Madison (NMRFAM) on Bruker DMX 600 and DMX 750 spectrometers equipped with three-axis gradients triple-resonance probes. Unless otherwise indicated, all data sets were collected at sample pH 2.5 and temperature 25 °C. [^{1}H−^{1}H]-TOCSY spectra used to follow the pH dependence of proton chemical shifts were acquired with mixing times of 50 ms; the TPPI mode was used for quadrature detection of the indirect dimension. Data sets collected for determining sequence-specific backbone and side chain assignments consisted of 2D ^{1}H NOESY, 2D $^1H_z{}^{15}N_z$-2 spin order exchange experiments, 3D HNCA, 3D HNCOCA, 3D HNCACB, 3D CCONH, 3D HNCO, 3D HCCH−COSY, 3D H(CCO)NH, and 3D ^{15}N TOCSY-HSQC. Distance constraints were based on four additional nuclear Overhauser enhancement (NOE) data sets, each collected with the mixing time t_m = 125 ms: 3D ^{15}N NOESY, 3D ^{13}C NOESY with ^{13}C carrier frequency in the aliphatic region, 2D ^{1}H NOESY in 90% H_2O/10% D_2O, and 2D ^{1}H NOESY in 100% D_2O. Care was taken to discriminate NOE cross-peaks from cross-peaks originating from direct chemical exchange or spin diffusion mediated by chemical exchange (*12*). An HNCO experiment with long-range coherence transfer was performed to obtain the $^{h3}J_{NC'}$ connectivities for detection of hydrogen bonds (*13*). ^{15}N transverse (R_2) relaxation data (*14*) were collected with the Bruker DMX750 spectrometer using relaxation delays of 0, 16, 32, 64, 96, 144, 192, and 240 ms.

NMR spectra were processed with either XWINNMR3.2 (Bruker, Billerica, MA) or FELIX95 (Molecular Simulations Inc., San Diego, CA) software. All ^{1}H dimensions were referenced directly to internal DSS, and ^{13}C and ^{15}N dimensions were referenced indirectly to DSS (*15*). Sparky software (http://www.cgl.ucsf.edu/home/sparky) was used in assigning and analyzing NMR spectra. The parameter-fitting module of Sparky was used to determine ^{15}N R_2 relaxation parameters by fitting peak intensities determined at different relaxation delays.

Structural Calculation and Structural Analysis. The simulated annealing protocol of the torsion angle dynamics program DYANA (*16*) was used in calculating all structures. Peak lists from the three aforementioned NOESY spectra, containing a total of 2 614 NOE cross-peaks for the *C* state and 2 505 NOE cross-peaks for the *T* state, were generated by manual peak picking with the program Sparky. NOE intensities were converted into upper distance bounds with the CALIBA function of DYANA. Additional NOE con-

straints were added in each preliminary round of calculations, and restraints that were consistently violated were rechecked by examining the spectra and removed if assignments proved to be incorrect. Constraints representing nine hydrogen bonds deduced from $^{h3}J_{NC'}$ HNCO data were included in the input data for both the *C* and *T* states (see Table S1 of the Supporting Information). Additional hydrogen bonds (4 for the *C* state and 3 for the *T* state) were deduced from the titration shifts of amide protons (*17*); constraints representing these were included in the input data for the respective structure determinations. Constraints representing ranges of ϕ and ψ dihedral angles (54 for the *C* state and 48 for the *T* state), generated from $^1H^\alpha$, $^{13}C^\alpha$, $^{13}C^\beta$, $^{13}C'$, and ^{15}N secondary shifts by the program TALOS (*18*), were included in later rounds of refinement. TALOS constraints were used only when nine out of 10 predicted values were clustered. In addition, six upper-bound and six lower-bound distance constraints were introduced to represent the three disulfide bridges: (P_{11}-Cys^8−P_{20}'-Cys^{38}, P_3-Cys^{16}−P_{17}'-Cys^{35}, and P_6'-Cys^{24}−P_{39}'-Cys^{56}). For reasons discussed below, the P_8-Tyr^{11}−P_7-Pro^{12} peptide bond was set to cis in the *C* state and trans in the *T* state. For structural analysis and evaluation, 20 conformers with the lowest target function values were selected from the final 50 structures calculated. The mean structure, calculated with MOLMOL software (*19*) from the ensemble of 20 best structures, was minimized in DYANA using 300 steps of variable target function minimization.

Kinetics and Thermodynamics of the Interconversion. [^{1}H−^{15}N]-two-spin-order exchange experiments (*20*) were carried out with samples at pH 2.5 at five temperatures (25, 30, 35, 40, and 45 °C) to determine the temperature dependence of the equilibrium. A procedure proposed by Otting et al. (*20*) was used to measure the exchange rate constants. [^{1}H−^{15}N]-two-spin-order exchange spectra were recorded at different temperatures under a range of mixing times: at 25 °C with τ_{mix} = 80, 100, 120, 140, and 160 ms; at 30 °C with τ_{mix} = 30, 40, 50, 60, 70, and 90 ms; at 35 °C with τ_{mix} = 40, 60, 80, and 90 ms; at 40 °C with τ_{mix} = 20, 30, 40, 60, and 80 ms; and at 45 °C with τ_{mix} =30 and 50 ms. The exchange rate constants were determined from the initial buildup rates of the exchange cross-peaks in the difference spectra, $\Delta I/\Delta\tau_{mix}$, and the intensities of the direct correlation peaks at zero mixing time, I_0. At zero mixing time:

$$k = \Delta I/(I_0 \Delta\tau_{mix}) \quad (1)$$

Instead of recording a separate experiment with zero mixing time, I_0 was obtained by extrapolation from the data recorded at short mixing times. Activation free energies $\Delta G^\ddagger$ were determined from measurement of the exchange rate constant *k* at various temperatures *T*, according to the Eyring relation:

$$\frac{\Delta G^\ddagger}{T} = -R\left(\ln k + \ln \frac{h}{\kappa k_B T}\right) \quad (2)$$

where k_B denotes the Boltzmann constant, *h* the Planck constant, and κ the transmission coefficient, which was assumed to be unity over the entire temperature range investigated. $\Delta G^\ddagger/T$ for the whole molecule was measured by averaging values determined from a number of individual peaks. The activation enthalpies $\Delta H^\ddagger$ and activation entropies $\Delta S^\ddagger$ were determined from eq 3:

$$\frac{\Delta G^\ddagger}{T} = \frac{\Delta H^\ddagger}{T} - \Delta S^\ddagger$$

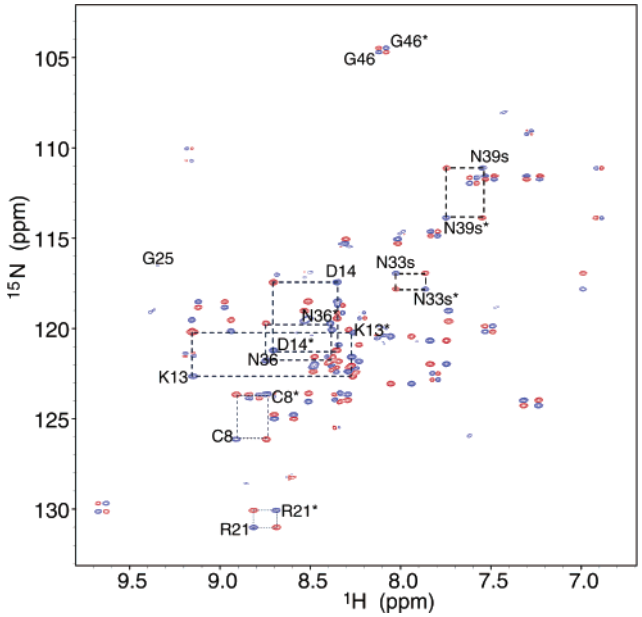

FIGURE 2: [^{1}H−^{15}N]-two-spin-order-exchange difference spectra of P_5-Pro^{14}Asp OMTKY3 at pH 2.5. The direct peaks (blue) for the *C* and *T* states are connected to one another by exchange cross-peaks (red). Resonances from the *T* form are identified by an asterisk; those from the *C* form have no designator. An "s" following N33 or N39 indicates that the marked peaks are from the side chain $^1H^\delta$atoms.

RESULTS

From analysis of [^{1}H−^{1}H]-TOCSY spectra of several OMTKY3 variants, P_5-Pro^{14}Asp OMTKY3 was chosen for structural studies because the *C* and *T* states of the protein were found to be stable and equally populated at pH 2.5.

Resonance Assignments for P_5-Pro^{14}Asp OMTKY3. [^{1}H−^{15}N]-two-spin-order-exchange experiments were used to cross-assign ^{1}H and ^{15}N resonances from individual atoms in two states of the protein. Blue contours (Figure 2) are direct cross-peaks observed in a normal [^{1}H−^{15}N]-HSQC spectrum. Red contours are exchange cross-peaks, which have negative intensities relative to the direct cross-peaks; they connect pairs of direct cross-peaks (one from each of the two states) into a characteristic rectangular pattern. Exchange peaks were observed for a number of backbone amides plus the side chain amides of P_{15}'-Asn^{33}, P_{18}'-Asn^{36}, and P_{21}'-Asn^{39}. (The $^1H^{\delta2/\delta3}$ signals of P_{15}'-Asn^{33} are outside the spectral region shown in Figure 2.) Direct cross-peaks from residues unaffected by the conformational change, e.g., P_7'-Gly^{25} and P_8'-Ser^{26}, are greatly suppressed in the difference spectrum. Suppression of direct cross-peaks in the difference spectrum helped to resolve exchange peaks with small chemical shift differences, for example, those from P_{28}'-Gly^{46} (Figure 2). The results of this experiment clearly demonstrate that the peak doubling arises from a dynamic conformational equilibrium, rather than from a covalent change such as deamidation. The assigned [^{1}H, ^{15}N]-HSQC spectrum of P_5-Pro^{14}Asp OMTKY3 at pH 2.5 is provided in the Supporting Information (Figure S1).

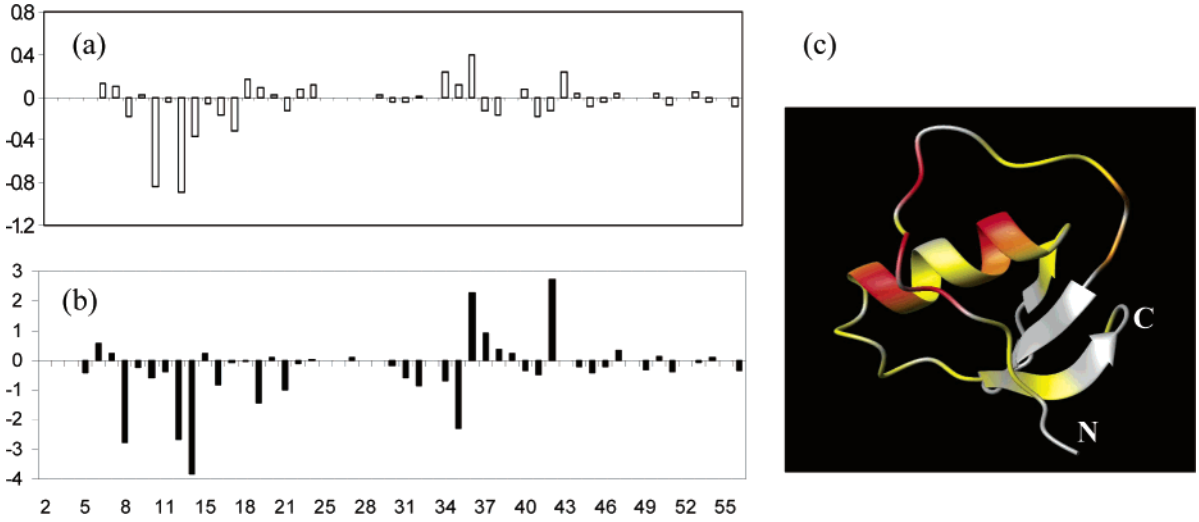

FIGURE 3: Chemical shift differences between the *C* (cis P_8-Tyr^{11}−P_7-Pro^{12} peptide bond) and *T* (trans P_8-Tyr^{11}−P_7-Pro^{12} peptide bond) conformers of P_5-Pro^{14}Asp OMTKY3 derived from the [^{1}H−^{15}N]-HSQC spectrum at pH 2.5: (a) differences in ^{1}H chemical shifts, (b) differences in ^{15}N chemical shifts, (c) weighted average chemical shift differences for ^{1}H and ^{15}N mapped onto the solution structure of OMTKY3 (*32*), with residues having Δ_{avg}(NH) of less than 0.1 ppm in gray, Δ_{avg}(NH) between 0.1 and 0.3 ppm in yellow, Δ_{avg}(NH) between 0.3 and 0.5 ppm in orange, and Δ_{avg}(NH) > 0.5 ppm in red. See the text for the definition of Δ_{avg}(NH). The N and C termini are indicated.

Assignments of the backbone $^1H^N$, $^1H^\alpha$, $^{13}C^\alpha$, ^{13}C, and ^{15}N resonances for the two states were completed by analyzing HNCA, HNCOCA, HNCO, H(CCO)NH, and [^{1}H, ^{15}N]-HSQC data from double-labeled samples at pH 2.5. HNCACB, CCONH, ^{15}N TOCSY-HSQC, and HCCH-COSY data were used in assigning side chain ^{1}H and ^{13}C resonances. Side chain $^{13}C^\gamma$ signals from Asn residues were assigned by reference to HNCO data collected with the dephasing and rephrasing times optimized for coherence transfer between the protons and nitrogen of each side-chain amide. The aromatic side chain ^{1}H resonances were assigned from the 2D NOESY spectrum of a sample in D_2O, on the basis of observed NOE cross-peaks between the aromatic protons and the aliphatic protons in the same residue. Resonances were assigned to specific states on the basis of observed scalar connectivities and NOE connectivities. A [^{1}H, ^{15}N]-HSQC spectrum of a sample at pH 4.0 was collected to confirm the identities of specific resonances in the *C* state, which is more highly populated at this pH. Assignments for the *C* state were consistent, for the most part, with those reported earlier for OMTKY3 under different conditions of pH and temperature (*21*−*23*). The assigned chemical shifts have been deposited at BMRB and are also available from the Supporting Information (Tables S2 and S3).

Evidence that the C and T States Differ by Prolyl Peptide Bond Isomerization. Multiple lines of evidence led to the conclusion that the two states differ by the configuration of the P_8-Tyr^{11}−P_7-Pro^{12} peptide bond. The fact that the residues with the largest chemical shift deviations are adjacent to P_7-Pro^{12} (Figure 3) provided the first suggestion that this residue might be involved. This hypothesis was strengthened by results of NMR investigations of the double mutant (P_7-Gly^{12}, P_5-Asp^{14}) OMTKY3, in which the proline presumed to undergo cis/trans isomerization had been mutated to glycine. Residues of wild-type OMTKY3 (or of single P_5-variants) that gave rise to doubled peaks showed single peaks in [^{1}H−^{1}H]-TOCSY of (P_7-Gly^{12}, P_5-Asp^{14}) OMTKY3 at pH 2.3 (see Figure S2 of the Supporting Information).

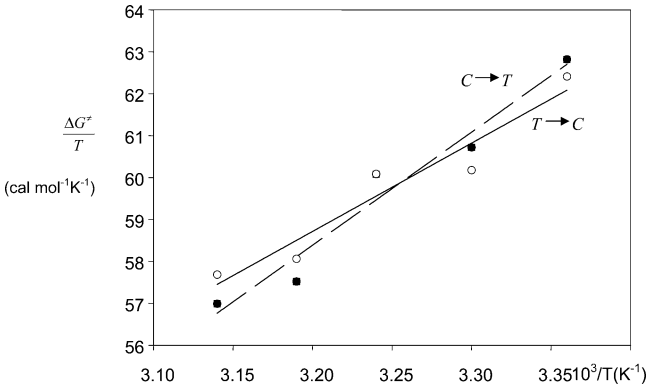

FIGURE 4: Plots of $\Delta G^\ddagger/T$, the free energy of activation divided by the absolute temperature, vs $1/T$, the reciprocal of the absolute temperature, for the ($C \rightarrow T$) conversion (black symbols), and the ($T \rightarrow C$) conversion (open symbols), where *C* indicates the state of P_5-Pro^{14}Asp OMTKY3 with cis P_8-Tyr^{11}−P_7-Pro^{12} peptide bond and *T* indicates the state with trans P_8-Tyr^{11}−P_7-Pro^{12} peptide bond. The lines represent least-squares fits each set of data points.

Prolyl peptide bond isomerizations are characterized by large positive activation enthalpies. The activation enthalpies for the C → T and T → C transitions of P_5-Pro^{14}Asp OMTKY3 were determined from measurements of the temperature dependence of the interconversion rates. The measured exchange rate constants varied from 0.25 s^{-1} at 25 °C to 2.1 s^{-1} at 45 °C. Figure 4 shows the plot of $\Delta G^\ddagger/T$ versus $1/T$. From these data one obtains $\Delta H^\ddagger = 27.9$ (± 3.8) kcal mol^{-1} and $\Delta S^\ddagger = 30.9$ (± 12.4) cal mol^{-1} K^{-1} for forward (C→T) reaction and $\Delta H^\ddagger = 21.7$ (± 4.0) kcal mol^{-1} and $\Delta S^\ddagger = 10.8$ (± 12.7) for reverse (T→C) reaction, where the errors (in parentheses) were determined from least-squares fitting. The activation enthalpy $\Delta H^\ddagger$ determined for the reaction is comparable to others reported for prolyl peptide bond isomerizations in model peptides and other proteins (*24*, *25*).

For a cis prolyl peptide bond, the distance between the H^α of the preceding residue and the H^α of the proline is shorter than the distance between the H^α of the preceding residue and the H^δ of the proline; for a trans peptide bond,

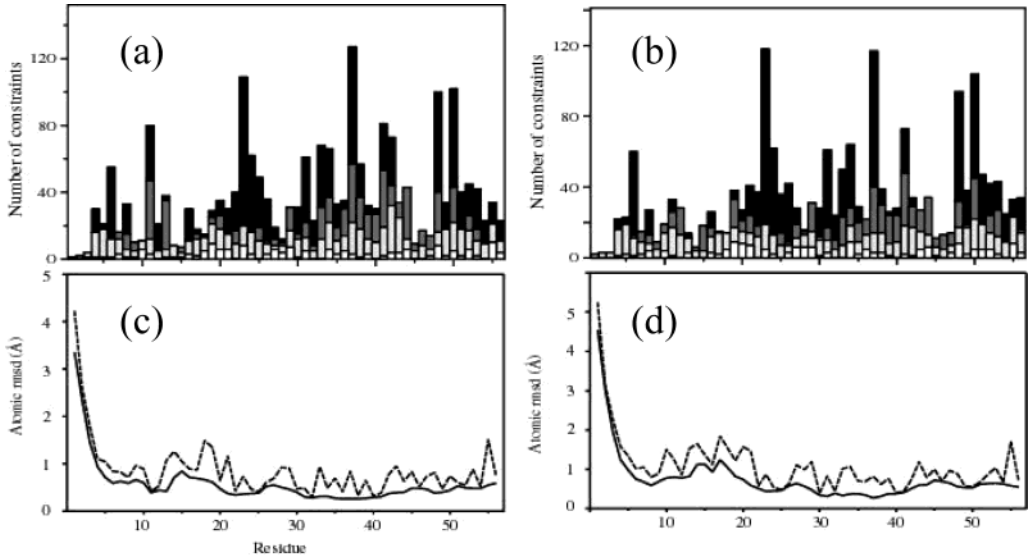

FIGURE 5: Summary of the numbers of structural constraints determined for the *C* (cis P_8-Tyr^{11}−P_7-Pro^{12} peptide bond) and *T* (trans P_8-Tyr^{11}−P_7-Pro^{12} peptide bond) states of P_5-Pro^{14}Asp OMTKY3 and the rmsd values of the family of conformers representing the structures. Number of NOE upper distance limits per residue plotted as a function of residue number for (a) the *C* state and (b) the *T* state. The numbers of intraresidue, sequential, medium, and long-range constraints are distinguished, respectively, as white, light gray, dark gray, and black bars. Average backbone (solid line) and heavy atom (dashed line) rmsd values are given for (c) the family of 20 *C*-state conformers and (d) the family of 20 *T*-state conformers.

these relative distances are reversed (*26*). Thus species with cis or trans prolyl peptide bonds can be distinguished on the basis of NOEs that report on these relative distances. [^{1}H−^{1}H]-NOESY data for P_5-Pro^{14}Asp OMTKY3 at pH 2.8 show an NOE between P_7-Pro^{121}H$^\alpha$ and P_8-Tyr^{11} ^{1}H$^\alpha$ (both from the *C* state), which identifies the peptide bond as cis, and NOEs between P_7-Pro^{12} ^{1}H$^\alpha$ and P_7-Pro^{14} ^{1}H$^{\delta 2}$ and ^{1}H$^{\delta 3}$ (all from the *T* state), which identify the peptide bond as trans (see Figure S3 of the Supporting Information).

Finally, cis and trans prolyl peptide bonds also can be distinguished on the basis of chemical shift comparisons. A prolyl $\delta^{13}C^\gamma$ generally is 1.5−2.0 ppm to higher frequency in the cis configuration than in the trans (*27*, *28*). Moreover, pairwise graphical comparisons of $\delta^{13}C^\beta$ and $\delta^{13}C^\gamma$ chemical shifts provide an additional statistic for distinguishing cis and trans Xaa−Pro peptide bond configurations (*29*). In the present case, the P_7-Pro^{12} chemical shifts for $^{13}C^\gamma$ in the *C* (24.4 ppm) and *T* states (27.3 ppm) are consistent with the P_8-Tyr^{11}−P_7-Pro^{12} peptide bond being cis in *C* and trans in *T*.

Structure Calculations. Prior to calculation of the final structures, the configuration of the P_8-Tyr^{11}−P_7-Pro^{12} peptide bond was constrained to be cis in the conformers representing the *C* state and trans in those representing *T*. The inverse configuration was tried with each set of input data (trans for *C* and cis for *T*), but these led to large numbers of constraint violations.

Starting with the NOE cross-peak lists, hydrogen bond constraints and disulfide bonds constraints for P_5-Pro^{14}Asp OMTKY3 described in Materials and Methods, the DYANA software package yielded 1,143 unique distance constraints for the *C* state and 1,063 for the *T*. Thus the average constraints per residue were 20.4 for *C* and 19.0 for *T*. The distributions of distance constraints for *C* and *T*, plotted as a function of residue number, are shown in Figure 5a,b. For both conformers, more constraints were distributed in the segments P_4'-Pro^{22}−P_{10}'-Asn^{28}, P_{12}'-Thr^{30}−P_{24}'-Val^{42}, and P_{30}'-Leu^{48}−P_{38}'-Cys^{56} than in other regions. No medium- or long-range NOEs were observed for the first three N-terminal residues. Many more constraints were found for P_8-Tyr^{11} in the *C* state (80) than in the *T* state (33).

The 20 conformers representing the *C* state are shown in Figure 6a, and those representing the *T* state are shown in Figure 6b. Structure statistics are summarized in Table 1. None of the 20 structures had NOE violations greater than 0.30 Å or any violations of van der Waals contacts.

Superposition of residues 6−56 for the final ensemble of 20 torsion angle dynamics conformers yielded root-mean-square deviations from the mean backbone structures of 0.58 Å (for the family of *C* conformers) and 0.75 Å (for the family of *T* conformers). The average backbone and heavy atom rmsd values relative to the mean structures of each conformer are shown as a function of residue number in Figure 5c,d. The atomic rms deviations for the N-terminal residues are relatively high in both conformers. Rmsd values for residues in the segment P_9-Glu^{10}−P_1-Leu^{18} were higher in the *T* state than in the *C* by 0.26−0.58 Å but were nearly equivalent elsewhere. The *C* state more closely resembles structures of wild-type OMTKY3 determined at higher pH values (*30*−*33*).

Dependence of the Peptide Bond Configuration on pH. [^{1}H−^{1}H]-TOCSY spectra were collected from solutions of P_5-Pro^{14}Gly OMTKY3(6−56), P_5-Pro^{14}Ala OMTKY3(6−56), P_5-Pro^{14}Asp OMTKY3(6−56), and wild-type OMTKY3(1−56) at pH values ranging from neutral to acidic. Similar reversible pH-dependent conformational transitions were observed for all three variants. However, the number of residues with chemical shifts perturbed by the conformational transition was found to depend on the nature of the side chain of P_5-X^{14}. In P_5-Pro^{14}Ala OMTKY3(6−56), very few residues exhibited doubled peaks. However, in P_5-Pro^{14}Gly OMTKY3(6−56) and P_5-Pro^{14}Asp OMTKY3(6−56), more than two-thirds of the residues were perturbed by the conformational transition.

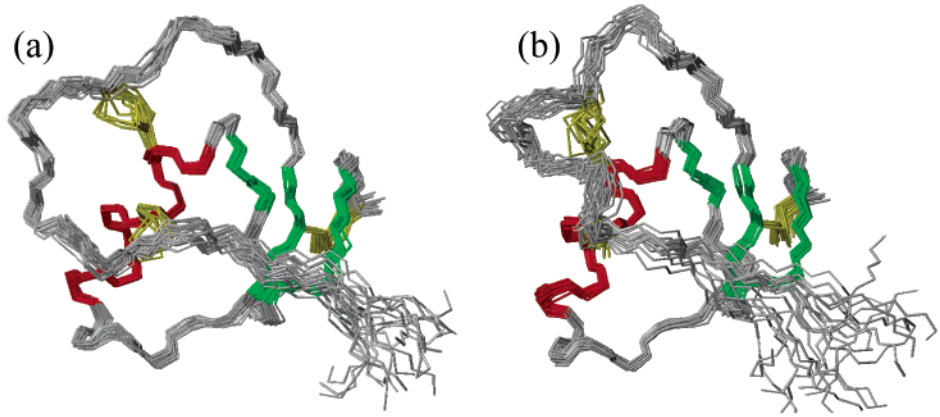

FIGURE 6: Representation of the structures of the two forms of P_5-Pro^{14}Asp OMTKY3 present in solution at pH 2.5: (a) the *C* state with cis P_8-Tyr^{11}−P_7-Pro^{12} peptide bond and (b) the *T* state with trans P_8-Tyr^{11}−P_7-Pro^{12} peptide bond. Each structure is represented by a superposition of the 20 conformers with lowest target functions from 50 calculated in the last round of refinement. Disulfide bridges are shown in yellow, β-strands in green, and α-helices in red.

Table 1: Statistics for the Three-Dimensional Structures of the *C* and *T* States of P_5-Pro^{14}Asp OMTKY3

parameters	*C* state (cis P_8-Tyr^{11}−P_7-Pro^{12} peptide bond)	*T* state (trans P_8-Tyr^{11}−P_7-Pro^{12} peptide bond)
NOE Constraints		
long	474	431
medium	236	218
short	272	252
intraresidue	163	163
Ramachandran Statistics		
most favored	73.3	70.7
additional allowed	23.5	24.1
generously allowed	2.6	4.0
disallowed	0.5	1.2
target function		
family	0.38 ± 0.07	0.20 ± 0.05
minimized average	0.19	0.31
upper limit violations		
number > 0.1 Å	6 ± 2	3 ± 2
sum of violations (Å)	2.1 ± 0.4	1.7 ± 0.3
maximum violation (Å)	0.19 ± 0.02	0.15 ± 0.04
Van der Waals violations		
number > 0.1 Å	0 ± 0	0 ± 0
sum of violations (Å)	1.5 ± 0.2	1.0 ± 0.2
maximum violation (Å)	0.16 ± 0.04	0.10 ± 0.03
Rmsd (6−56) to the Mean Coordinates, Å		
backbone	0.58 ± 0.12	0.75 ± 0.18
heavy atom	1.15 ± 0.16	1.39 ± 0.20

The intensities of pairs of NMR peaks in the [^{1}H-^{1}H]-TOCSY data from a given variant at different pH values were integrated to obtain the relative occupancies of each conformer. Figure 7 shows the pH dependence of the relative populations of the *T* states of four P_5 variants of OMTKY3(6−56): Pro (wild-type), Ala, Asp, and Gly. All four variants showed similar peak doublings for residues P_4-Ala^{15}, P_6'-Cys^{24} (except for wild-type which showed no doubling), P_{22}'-Ala^{40}, and P_{23}'-Val^{41}, even though some of these residues (e.g., P_4-Ala^{15} and P_{23}'-Val^{41}) are spatially distant from one another (*33*). The four variants showed different mole fractions of the *T* state at the high and low pH extremes studied: ∼0.2 to ∼0.6 for P_5-Pro^{14}Asp, ∼0.2 to ∼0.7 for P_5-Pro^{14}Gly, ∼0.05 to ∼0.3 for P_5-Pro^{14}Ala, and ∼0 to ∼0.2 for wild type. All three showed transition midpoints near pH 3. The nonsigmoidal nature of the transition made it difficult to determine accurate pH_{mid} values.

For comparison purposes, [^{1}H−^{1}H]-TOCSY spectra were collected from two additional variants (data not shown): P_5-Pro^{14}Glu OMTKY3(6−56) and P_5-Pro^{14}His OMTKY3(6−56). The relative occupancies of *T* states in these two variants were both higher than that in wild-type OMTKY3 (6−56), but not as high as that in P_5-Pro^{14}Gly OMTKY3(6−56) or P_5-Pro^{14}Asp OMTKY3(6−56).

Mutants at P_1-Leu^{18} or P_6-Lys^{13}. The relative population of *T* state was found to be elevated when P_1-Leu^{18} was replaced by Gly^{18} (but not Ala^{18}) (see Figure S4 of the Supporting Information) or when P_6-Lys^{13} is replaced by Asp^{13} or Glu^{13}. The $^1H^N$ of P_6-Glu^{13} in the *C* state of P_6-Lys^{13}Glu OMTKY3 showed biphasic pH dependence (Figure 8a), as did the relative population of the *T* state with similar pH_{mid} values (Figure 8b). By contrast, the $^1H^N$ of P_6-Asp^{13} in the *C* state of P_6-Lys^{13}Asp OMTKY3 showed monophasic pH dependence (Figure 8c), as did the relative population of the *T* state with a similar pH_{mid} value (Figure 8d). These results suggest that the state of the P_6 residue is somehow coupled to the *C*/*T* transition.

Effect of the Conformational Transition on pK_a Values. The inherent high sensitivity of the [^{1}H−^{15}N]-HSQC experiment enabled us to follow peaks over the whole pH titration range and to determine the pK_a values for all six carboxyl groups in P_5-Pro^{14}Asp OMTKY3(6−56) in both the *C* and *T* conformational states. The pH titration results are presented in Table 2.

^{15}N Transverse Relaxation Measurements. The backbone ^{15}N R_2 relaxation rates for residues in the *C* and *T* states of P_5-Pro^{14}Asp OMTKY3 determined at 750.13 MHz (^{1}H frequency) at pH 2.5 and 25 °C are shown in Figure 9. As discussed above, the exchange rate between the two conformers under these conditions is 0.25 s^{-1}, which is much slower than the R_2 rates expected for a protein of this size (*34*). Thus, chemical exchange effects were expected to result in only minor errors in the experimental R_2 values for the two states.

DISCUSSION

Protein folds and stabilities, and hence functions, can be greatly altered by cis/trans isomerizations of prolyl peptide bonds or by changes in the conformations of disulfide bridges (*25*, *35*−*39*). Efforts have been made to explore how internal

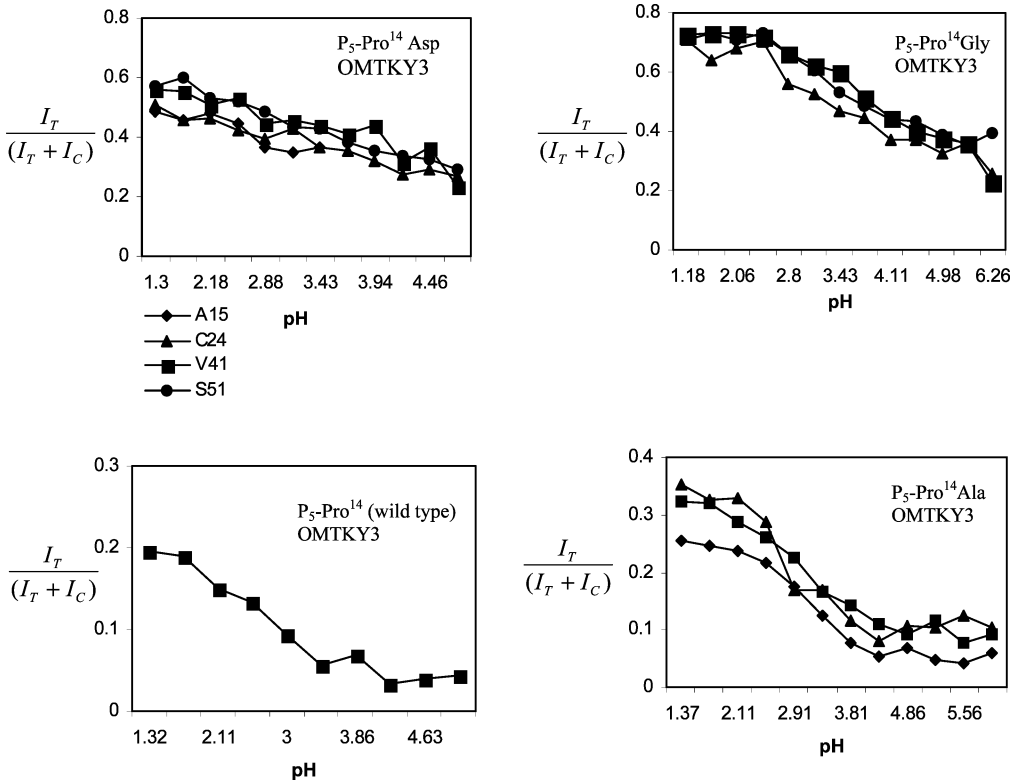

FIGURE 7: The pH dependences of the mole fraction of the low-pH conformer in OMTKY3 variants: P_5-Pro^{14} OMTKY3 (wild type), P_5-Pro^{14}Ala OMTKY, P_5-Pro^{14}Asp OMTKY3, and P_5-Pro^{14}Gly OMTKY3. Populations were determined from the relative volumes of [^{1}H−^{1}H]-TOCSY peaks corresponding to each state: $I_T/(I_T + I_C)$, where I_T and I_C refer to the intensities of peaks in the *T* state and *C* state, respectively.

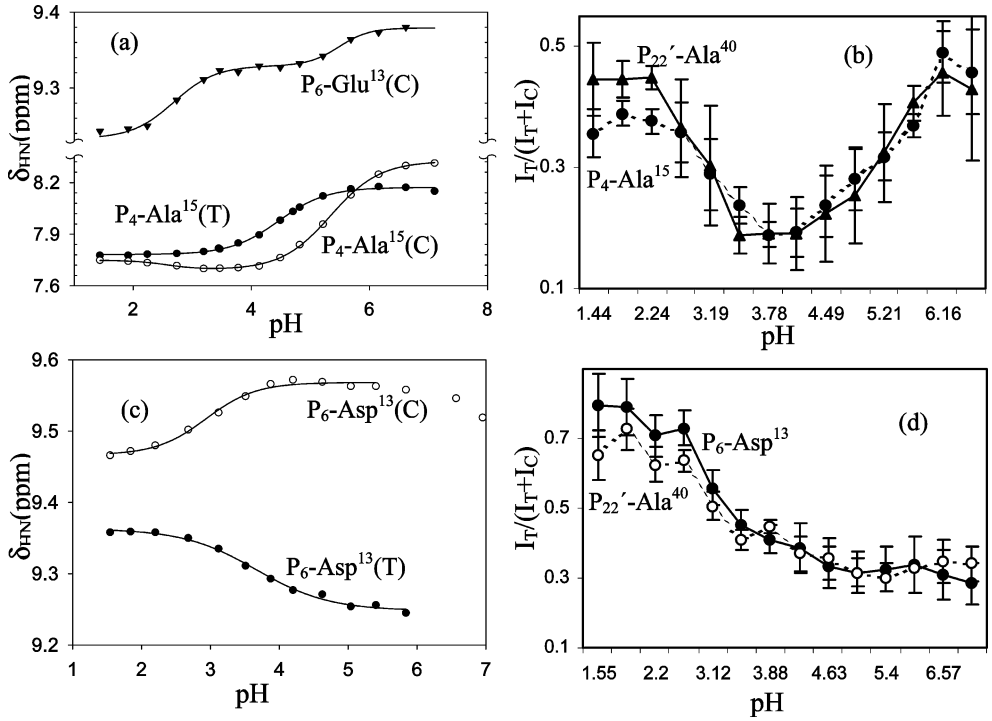

FIGURE 8: Effects of pH on P_6-Lys^{13}Asp/Glu OMTKY3: (a) Titration curves for $^1H^N$ signals from P_6-Glu^{13} and P_4-Ala^{15} in the *C* state of P_6-Lys^{13}Glu OMTKY3. (b) Relative populations of the *T* state as a function of pH for P_6-Lys^{13}Glu OMTKY3. (c) Titration curves for $^1H^N$ signals from P_6-Asp^{13} in the *C* and *T* states of P_6-Lys^{13}Asp OMTKY3. (d) Relative populations of the *T* state as a function of pH for P_6-Lys^{13}Asp OMTKY3. Curves in panels a and c represent best fits to theoretical titration equations. Error estimates in panels b and d were derived from the noise of the spectra.

dynamics, hydrophobic, and electrostatic effects in proteins influence the relative populations of isoforms (*20*, *26*, *40*−*45*). In this regard, advanced NMR techniques provide an effective approach for identifying conformational equilibria (*14*, *20*, *46*), as well as for determining the structural and dynamic features of each conformer (*29*, *47*).

Comparison of the Structures of the C and T States with that of Wild-Type OMTKY3. Several NMR and X-ray

Table 2: Titration Parameters[a]

	P_{12}-Asp[7]		P_9-Glu[10]		P_5-Asp[14]		P_1'−Glu[19]		P_9'−Asp[27]		P_{25}'−Glu[43]		Cys56 (P_{38}')	
	C	T	C	T	C	T	C	T	C	T	C	T	C	T
pK_a	2.83 (±0.11)	3.34 (±0.07)	4.27 (±0.05)	4.05 (±0.08)	3.76 (±0.03)	3.66 (±0.06)	3.40 (± 0.06)	3.71 (±0.07)	2.22 (±0.04)	2.22 (±0.04)	4.90 (±0.08)	4.58 (±0.10)	2.27 (±0.05)	2.27 (±0.07)
Hill coefficient	0.69 (±0.08)	0.75 (±0.09)	0.88 (±0.08)	0.57 (±0.07)	1.04 (±0.07)	0.91 (0.11)	1.16 (±0.17)	1.07 (±0.18)	0.92 (±0.05)	0.92 (±0.05)	0.77 (± 0.08)	0.63 (±)0.08	0.86 (±0.04)	0.81 (±0.05)

[a] Derived from the pH dependence of ^{15}N NMR signals from six residues of P_5-Pro[14]Asp OMTKY3 in the *C* and *T* states.

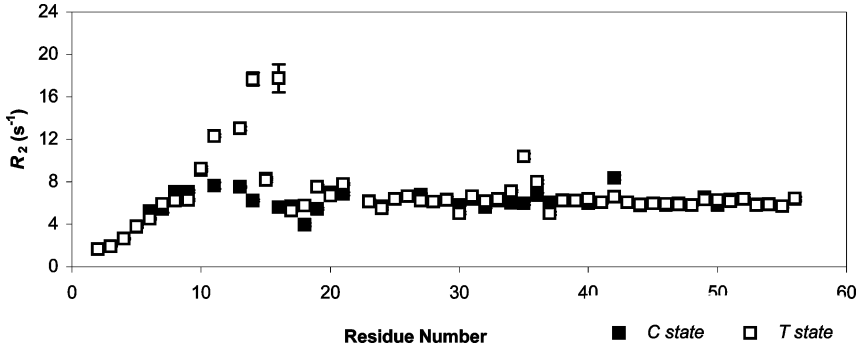

FIGURE 9: Comparison of ^{15}N R_2 relaxation rates plotted as a function of the amino acid sequence for the two states of P_5-Pro[14]Asp OMTKY3 at pH 2.5. The error bars represent standard deviations returned upon nonlinear analysis of the relaxation data.

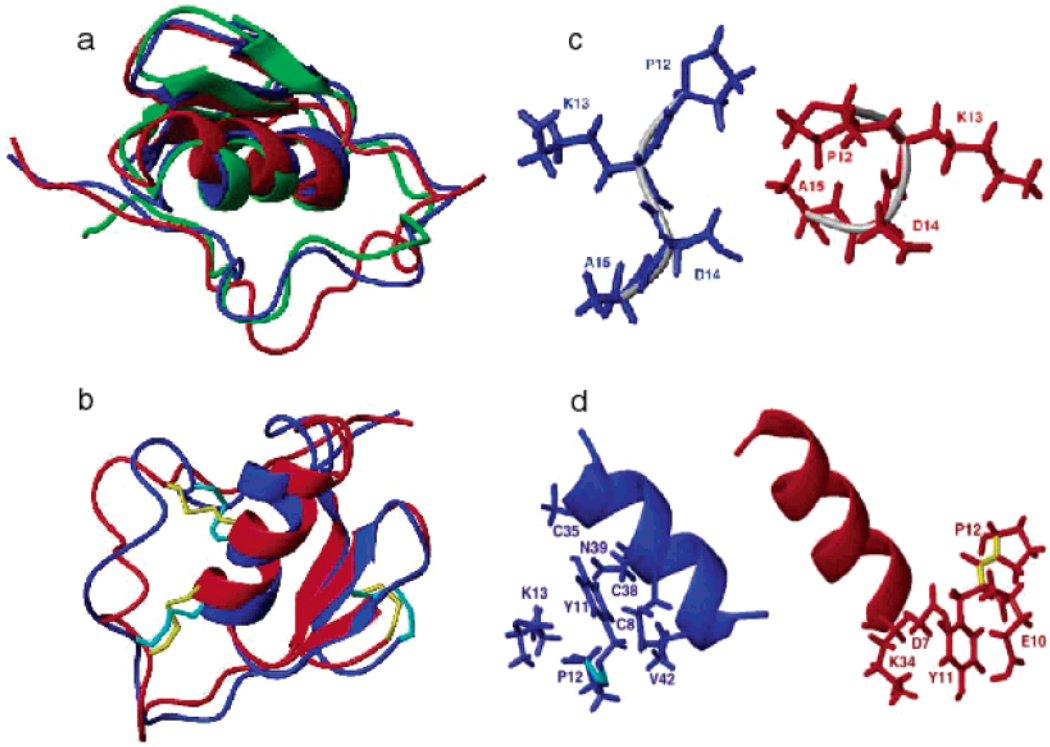

FIGURE 10: Comparisons of the structures of the *C* and *T* forms of P_5-Pro[14]Asp OMTKY3 at pH 2.5. (a) *C* state structure (in blue) and *T* state structure (in red) compared with the structure of wild-type OMTKY3 (in green) determined at pH 4.1 (*32*). (b) Superposition of the mean structures of the *T* state (in red) and the *C* state (in blue). The disulfide bridges in the *C* state are shown in cyan; those in the *T* state are shown in yellow. (c) Detailed view of main chain conformations and side chain packing of residues from P_7-Pro[12] to P_4-Ala[15] in the *C* (left, in blue) and *T* states (right, in red). (d) Comparison of the region of the P_8-Tyr[11]−P_7-Pro[12] peptide bond in the *C* state (left, in blue) and *T* state (right, in red). P_8-Tyr[11]−P_7-Pro[12] peptide bond is shown in cyan in the *C* state and yellow in *T* state. Residues making contacts with the P_8-Tyr[11] ring in each state are shown in the same color as the backbone ribbon.

structures are available for wild-type OMTKY3 (*30*−*33*, *48*). Comparison is made here (Figure 10a) between the mean structures of the *C* and *T* states of P_5-Pro[14]Asp OMTKY3 and that of wild-type OMTKY3 determined by NMR at pH 4.1 (*33*). The three-stranded β-sheet is the most conserved core element in the three structures, with no greater than 0.6 Å backbone rmsd between OMTKY3 and *C* or *T*. The region exhibiting the largest differences is the reactive-site loop of the *T* state. The backbone rmsd values between the reactive-site loop of wild-type OMTKY3 (P_{13}-Val[6]−P_3'-Arg[21]) and the corresponding loops of the *T* state and *C* state are 2.7 and 1.1 Å, respectively. The backbone of the reactive site loop of *T* diverges significantly from the highly conserved backbone of OMTKY3 and other members of the

Table 3: Angles Specifying the Conformation of the Backbone of the Reactive Site Region

	P_6	P_5	P_4	P_3	P_2	P_1	P_1'	P_2'	P_3'
	ϕ, ψ	ϕ, ψ	ϕ, ψ	ϕ, ψ	ϕ, ψ	ϕ, ψ	ϕ, ψ	ϕ, ψ	ϕ, ψ
wild-type OMTKY3 *C* state	−118, 144	−89, 14	−165, 121	−101, 134	−55, −163	−117, −12	−46, 153	−97, 93	−122, 84
P_5-Asp[14]OMTKY3 *C* state	−97, 147	−86, 19	−153, 169	−144, 173	−101, 156	−92, −23	−60, 151	−106, 117	−141, 99
P_5-Asp[14]OMTKY3, *T* state	−64, −18	−85, −11	−116, 85	176, 83	−96, −149	−65, −11	−67, 111	−109, 121	−138, 109

family of canonical proteinase inhibitors (*3*, *31*, *49*−*53*). Although similar in the $P_2'-P_3'$ region, large local conformational differences are observed in P_6-P_1 region. In particular, the backbone torsion angles of P_6 (Lys13) and P_5 (Asp14) in *T* are more characteristic of a 3_{10}-helix, whereas they are more extended in wild-type OMTKY3. In addition, the α-helix in *T* deviates from its alignment in *C* and wild-type OMTKY3, owing to reasons discussed below.

The local structure of the *C* state of P_5-Asp OTMKY3 at pH 2.5 is similar to that of wild-type OMTKY3 at pH 4.0 (*32*) (Table 3), with the exception of a small deviation in the region P_4-P_2, which presumably results either from the pH difference or the P_5 residue substitution. This structural comparison is further supported by the chemical shift comparison of wild-type OMTKY3 with the two states of P_5-Asp OMTKY3 (see Figure S5 of the Supporting Information).

Structural Differences between the C and T States. The minimized mean structures for the two states are compared in Figure 10b. The *C* and *T* states share similar structural elements, such as the three-stranded antiparallel β-sheet and the β-turn connecting strands β_1 and β_2. Although the overall backbone rms deviation between the mean structures of *C* and *T* is 3.03 Å, the backbone rms deviation of the β-sheet in the two is only ∼0.26 Å. The α-helix is also preserved in the two states (backbone rmsd 0.34 Å) with the largest difference being in the orientation of the two ends of the helix. Most of the hydrogen bonds stabilizing the β-sheet and the α-helix are also present in both states (see Table S1 of the Supporting Information). The side chain of P_1-Leu[18] has a similar orientation in the *C* and *T* states, highly exposed to the solvent in both.

The side chains of P_7-Pro[12] and P_4-Ala[15] are farther apart in *C* than in *T* (Figure 10c). In the *C* state, the side chain of P_{24}'-Val[42] and the P_7-Pro[12] ring make many hydrophobic contacts. As a result in the *C* state, the P_7-Pro[12]−P_4-Ala[15] backbone is rather extended. In the *T* state, as a consequence of disruption of the hydrophobic interactions between P_7-Pro[12] and P_{24}'-Val[42], the side chain of P_7-Pro[12] projects away from the helix and becomes closely packed with the side chain of P_4-Ala[15] (Figure 10c). Concurrently, the side chain of P_6-Lys[13], which contacts the side chain of P_{21}'-Asn[39] in *C* state, moves closer to the side chains of P_5-Asp[14] and other residues within the reactive-site loop.

Relocation of the Tyr-11 Ring. The aromatic ring of P_8-Tyr[11] moves from the center of the α-helix in *C* to the N-terminus of the helix in *T*. This relocation of the phenyl ring disrupts the hydrophobic cluster of the *C* state and loosens the contacts between the reactive-site loop and the α-helix. As shown in Figure 10d, the relocated P_8-Tyr[11] ring in *T* contacts several other residues, including P_{12}-Asp[7], P_4-Ala[15], and P_{16}'-Lys[34]. In addition, relocation of the P_8-Tyr[11] ring results in large structural perturbations of residues in the loop containing the P_8-Tyr[11]−P_7-Pro[12] peptide bond as well as in the N- and C-terminal residues of the α-helix. Our structural analysis suggests that the aromatic ring of P_8-Tyr[11] plays a vital role in stabilizing the cis conformation of the peptide bond. In the *C* state, the aromatic ring of P_8-Tyr[11] is attached to the middle of the α-helix, with its plane parallel to the axis of the helix (Figure 10c). The hydrophobic ring of P_8-Tyr[11] makes many contacts with the side chains of surrounding residues (P_{11}-Cys[8], P_6-Lys[13], P_{17}'-Cys[35], P_{20}'-Cys[38], P_{21}'-Asn[39], and P_{24}'-Val[42]). The relative spatial arrangement between the reactive-site loop and the helix is stabilized further by packing between the ring of P_7-Pro[12] and the side chain of P_{24}'-Val[42].

Differences in Hydrogen Bonding. In the *C* states of wild-type OMTKY3 (*5*) and P_5-Asp OMTKY3, H^N of P_2-Thr[17] exhibits a negative titration shift (to lower frequency with increasing pH), which has been attributed to the hydrogen bond between the side chains of P_2-Thr[17] and P_1'-Glu[19] (*5*). In the *T* state, however, the H^N of P_2-Thr[17] exhibits a positive titration shift. This result is indicative of a difference in hydrogen bonding between P_2-Thr[17] and P_1'-Glu[19] in *C* and *T*. Coupling between the change in peptide bond configuration at P_8-Tyr[11]−P_7-Pro[12] and the change in hydrogen bonding at P_2-Thr[17] and P_1'-Glu[19] probably is mediated by changes in the contacts among P_2-Thr[17], P_{15}'-Asn[33], and P_{16}'-Lys[34], which are present in *C* but disrupted in *T*. Structural comparison of the two states also reveals that a hydrogen bond between the amide group of P_4-Ala[15] and the backbone oxygen of P_7-Pro[12] exists in *T* but not in *C*.

Differences in the Conformations of Two Disulfide Bridges. Of the three disulfides the $^{13}C^{\alpha}$ and $^{13}C^{\beta}$ resonances of two (P_{11}-Cys[8]−P_{20}'-Cys[38] and P_3-Cys[16]−P_{17}'-Cys[35]) showed large chemical shift perturbations (>|0.5 ppm|). The side chain resonances of the third disulfide bridge (P_6'-Cys[24]−P_{38}'-Cys[56]) exhibited no chemical shift perturbations. Disulfide bridge P_6'-Cys[24]−P_{38}'-Cys[56] is well defined, with a right-handed conformation in both the *C* and *T* states. Although the conformations of the other two disulfide bridges are less clearly defined, comparison of the structures for *C* and *T* (Figure 6) shows that these two disulfides adopt very different conformations in the two forms. The $C^{\alpha}-C^{\alpha}$ distances for each of these is longer by >1 Å in *T* than in *C*. Since these two disulfides covalently bond the reactive-site loop to the α-helix, the changes in their geometries probably arise from strains imposed by the structural rearrangement of this region of the protein.

Factors Contributing to Differential Stabilization of the C and T States. It has been recognized that an aromatic residue preceding a proline can have a large effect on the relative stabilities of the cis and trans peptide bond configurations (*42*, *54*, *55*). Surveys of the Protein Data Bank by MacArthur et al. (*56*) indicated that a cis peptide bond is more prevalent in Xxx−Pro peptide bonds when Xxx is an aromatic residue. From NMR investigations of cis/trans isomerization of the model peptide acetyl-Gly-Xxx-Pro-Gly

carboxamide, where Xxx = Tyr, Phe, Trp, etc., Wu and Raleigh suggested that interactions between the aromatic ring and the prolyl ring stabilize the cis state of the Xxx−Pro peptide bond (*57*). The present results show how the packing of the aromatic ring of P_8-Tyr^{11} with residues in the α-helix play a vital role in stabilizing the cis conformation of the P_8-Tyr^{11}−P_7-Pro^{12} peptide bond.

How can the structural results rationalize the experimental order of stabilization of the trans state in P_5-Pro^{14}Xxx OMTKY3 mutants: Xxx = Gly > Asp > Glu > Ala > His > Pro? Analysis suggests that the presence of C^{β} and C^{δ} substituents on residue 14 interfere with the packing between the side chains of P_7-Pro^{12} and P_4-Ala^{15} in the *T* state (Figure 10c). This may explain why replacement of P_5-Pro^{14} by Gly greatly elevates the population of the *T* state and why the *C* state predominates in wild-type OMTKY3, P_5-Pro^{14}Ala OMTKY3, and P_5-Pro^{14}His OMTKY3. This kind of steric argument, however, fails to explain why the *T* state is favored when residue 14 is Asp or Glu. Thus a second mechanism must be invoked. A plausible mechanism is stabilization of *T* by electrostatic interaction between the side chain of P_6-Lys^{13} and the acidic side chain at residue P_5-Asp/Glu^{14}.

A precedent for such a dual mechanism comes from work of Hodel et al. (*58*) on the configuration of the Lys^{116}-Pro^{117} peptide bond of staphylococcal nuclease (SNase). In wild type SNase, the cis form is much more highly populated than the trans form (*26*, *58*). Replacement of Lys^{116} by Gly, Asp, or Asn stabilizes the trans form relative to the cis form, whereas replacement by Ala, Met, or Gln has no effect on the equilibrium. These results were explained in terms of two distinct mechanisms: reduction of the steric barrier (in the case of Gly) and side-chain tertiary interactions (in the case of the Asp mutant).

Dependence of the C ⇄ T Equilibrium on pH. Between pH 5.0 and 1.3, $I_T/(I_T+I_C)$ changes from 0.22 to 0.55 (Figure 7); thus, $K = [T]/[C]$ changes from 0.28 to 1.2 over this pH range. This result suggests that the *T* state has a higher affinity for one or more protons than the C state. This effect can be modeled by a coupled equilibrium of the form shown in eq 4, where the acidic site(s) affected is represented in the *C* state as CA^- and in the *T* state as TA^-.

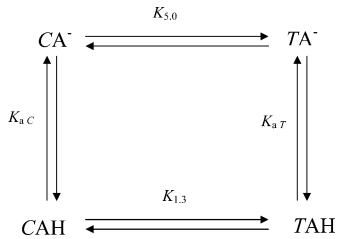

(4)

Because of the equilibrium condition, $pK_{a\,C} + pK_{5.0} = pK_{a\,T} + pK_{1.3}$. In addition, from the change in the cis/trans equilibrium noted above, $pK_{5.0} - pK_{1.3} = 0.63$. Thus, over this pH range, $\Delta pK_a = pK_{a\,T} - pK_{a\,C} = 0.63$.

The side chains of P_{12}-Asp^7 and P_1'-Glu^{19} showed higher pK_a values in the *T* than the *C* form (Table 2). The side chain of P_5-Asp^{14} and the *C*-terminal carboxyl P_{38}'-Cys^{56} had similar pK_a values in the two states. And the side chains of P_9-Glu^{10} and P_{25}'-Glu^{43} exhibited lower pK_a values in the *T* state than the *C* state. Not surprisingly, residues exhibiting large pK_a differences in *C* and *T* lie in regions with major chemical shift differences, whereas those with minimal pK_a difference lie in regions with minor shift differences (Figure 3). The data of Table 2 yield 21.62 as the sum of the six pK_a values for the *T* form and 20.98 as the sum of the six pK_a values for the *C* form. Thus, the aggregate $C \rightarrow T$ pK_a difference of 0.64 is in excellent agreement with the value of 0.63 predicted from the pH dependence of the cis/trans equilibrium.

To test this model, another double mutant, (P_{12}-Ala^7, P_5-Asp^{14}) OMTKY3, was constructed, and [^{1}H−^{1}H]-TOCSY data for this mutant were collected at pH 6.0 and 2.2 (Supporting Information, Figure S6). The spectra were assigned by reference to spectra of P_5-Asp^{14} OMTKY3. The pK_a of P_{12}-Asp^7 was determined to be 0.5 pH unit higher in the *T* state than in *C* state (Table 2). The expectation was that, in the absence of other effects of the mutation, removal of a titrating group with a positive $C \rightarrow T$ pK_a difference should stabilize the trans configuration of the P_8-Tyr^{11}−P_7-Pro^{12} peptide bond. Indeed, the double mutant exhibited the expected increased stabilization of *T*. The fractional occupancy of *T* in this mutant was 0.5−0.6 at pH 6.0 (vs 0.22 for the single mutant) and ∼0.7 at pH 2.2 (vs 0.5 for the single mutant).

In wild-type OMTKY3, the low pK_a of P_{12}-Asp7 has been attributed to a hydrogen bond between the side chains of P_{12}-Asp^7 and P_{10}−Ser^9 (*5*, *59*, *60*). This hydrogen bond is weakened in the *T* state compared the *C* as shown by the pH titration shift of the P_{10}−Ser^9 H^N (0.5 ppm in *C*, 0.3 ppm in *T*). A second factor contributing to the elevated pK_a of Asp7 in *T* compared to *C* may be the increased hydrophobic environment of the P_{12}-Asp^7 side chain in *T* (*9*, *61*−*65*). Structural comparison (Figure 10d) reveals relatively close contacts between the side chains of P_{12}-Asp^7 and P_8-Tyr^{11} in *T* state but not in *C*.

Results from pH titration studies of various OMTKY3 mutants indicate that the hydrogen bond between the side chains of P_1'-Glu^{19} and P_2-Thr^{17} lowers the pK_a of P_1'-Glu^{19} by 0.4−0.5 pH unit (*11*). Our structural and pH titration results suggest that the higher pK_a value observed for P_1'-Glu^{19} in *T* probably arises from the effect of breaking or weakening this hydrogen bond.

Comparison of the Two Low-pH Conformational Transitions: In 1967, Donovan reported a structural transition at low pH in whole chicken ovomucoid. A blue shift of the absorption spectrum was found to be accompanied by a 300% increase in fluorescence when chicken ovomucoid solutions were made acidic (*6*). These changes are reversible and have the pH dependence of a single acidic group of pK_a = 2.8. In later studies, March (*66*) assigned P_{13}'-Tyr^{31} as the residue in all three domains responsible for the change in the optical spectrum, and Croll (*67*) observed a transition with a pH_{mid} of about 2.5 that perturbed the chemical shifts of ^{13}C NMR signals of chicken ovomucoid third domain assigned to $^{13}C^{\gamma}$ and $^{13}C^{\zeta}$ of P_{13}'-Tyr^{31}. Both authors explained the spectral results in terms of protonation of the side chain of P_9'-Asp^{27} at low pH, which disrupts the hydrogen bond between the aromatic ring of P_{13}'-Tyr^{31} and the side chain of P_9'-Asp^{27}. The present studies show that the actual pK_a of P_9'-Asp^{27} is about 2.7 in both conformational states, a value that is close to the pH_{mid} for both the Donovan transition and for the $C \rightleftarrows T$ transition. Although the two transitions occur with similar pH_{mid} values, it appears

that they are independent. The P_8-Tyr^{11}−P_7-Pro^{12} cis/trans isomerization is slow on the NMR time scale and is characterized by a low Hill coefficient, whereas the residues affected by the Donovan transition show single peaks and a Hill coefficient close to unity (*67*).

Internal Dynamics of the Two States. The *C* and *T* states of P_5-Asp^{14} OMTKY are equally populated at pH 2.5, indicating that their free energies are equivalent. However, our structural analysis revealed that the $C \rightarrow T$ transition results in the loss of many hydrophobic contacts between the P_8-Tyr^{11} ring and other groups. How does the *T* state compensate for this energy loss? To address this question, we explored the dynamic features of the two states by measuring ^{15}N transverse relaxation.

As shown in Figure 9, the average ^{15}N R_2 relaxation rate for residues in *C* state is 6 s^{-1}, with the rates for the N-terminal residues much slower than average and those for the P_{11}-Cys^8−P_4-Ala^{15} loop residues slightly faster than average. Although the ^{15}N R_2 rates were similar in the two states for most residues, several residues exhibited much faster relaxation in *T* than in *C*: these included the stretches P_8-Tyr^{11}−P_3-Cys^{16} (except P_4-Ala^{15} and P_{16}'-Lys^{34}−P_{18}'-Asn^{36}. We attribute the increased ^{15}N R_2 relaxation rates for these residues to conformational exchange within the trans state on the μs to ms time scale within that state. If we assume that the exchange process within *T* is two-state (between states *T* and *T**), the overall exchange process is described as:

$$C \rightleftarrows (T \rightleftarrows T^*)$$

Although the origin of this slow exchange event remains unclear, the increased loop mobility undoubtedly contributes entropic stabilization to the *T* state.

Multiple exchange processes on different time scales reflect the complexity of the free energy landscape for the protein. A similar example was provided by an SH3 domain studied by Kay and co-workers (*14*, *47*), which exhibited both a conformational exchange between the folded and unfolded states, with a k_{ex} of 2.2 s^{-1}, and a more rapid exchange process on the microsecond−millisecond time scale within the unfolded state.

After this manuscript was submitted, a paper appeared by Hemmi et al. (*68*) describing a silver pheasant ovomucoid third domain variant containing an engineered disulfide bridge between cysteines mutated in at positions P_5 and P_{21}'. The inserted disulfide bride is homologous to one present in the ascidian trypsin inhibitor (*69*). Interestingly, in the context of the present study, the configuration of the P_8-Tyr−P_7-Pro peptide bond in the disulfide variant was determined to be trans (*68*), rather than cis as in wild-type silver pheasant ovomucoid third domain. The disulfide variant retained activity as a potent inhibitor of α-chymotrypsin and *Streptomyces griseus* proteases A and B but lost most of its activity as an inhibitor of porcine pancreatic elastase (*68*).

ACKNOWLEDGMENT

The authors thank Craig S. Newman and Yi-ping Zheng for assistance with preparation of the manuscript.

SUPPORTING INFORMATION AVAILABLE

Six figures and three tables as referenced in the text are available free of charge via the Internet at http://pubs.acs.org.

REFERENCES

1. Schechter, I., and Berger, A. (1967) *Biochem. Biophys. Res. Commun. 27*, 157−162.
2. Laskowski, M., Jr., and Kato, I. (1980) *Annu. Rev. Biochem. 49*, 593−626.
3. Bode, W., and Huber, R. (1992) *Eur. J. Biochem. 204*, 433−451.
4. Lineweaver, H., and Murray, C. W. (1947) *J. Biol. Chem. 171*, 565−581.
5. Schaller, W., and Robertson, A. D. (1995) *Biochemistry 34*, 4714−4723.
6. Donovan, J. W. (1967) *Biochemistry 6*, 3918−3927.
7. Choe, S. (1997) Ph.D. Thesis, University of Wisconsin−Madison, Madison, WI.
8. Lu, S. M., Lu, W., Qasim, M. A., Anderson, S., Apostol, I., Ardelt, W., Bigler, T., Chiang, Y. W., Cook, J., James, M. N., Kato, I., Kelly, C., Kohr, W., Komiyama, T., Lin, T. Y., Ogawa, M., Otlewski, J., Park, S. J., Qasim, S., Ranjbar, M., Tashiro, M., Warne, N., Whatley, H., Wieczorek, A., Wieczorek, M., Wilusz, T., Wynn, R., Zhang, W., and Laskowski, M., Jr. (2001) *Proc. Natl. Acad. Sci. U.S.A. 98*, 1410−1415.
9. Qasim, M. A., Lu, S. M., Ding, J. H., Bateman, K. S., James, M. N. G., Anderson, S., Song, J. K., Markley, J. L., Ganz, P. J., Saunders, C. W., and Laskowski, M., Jr. (1999) *Biochemistry 38*, 7142−7150.
10. Hinck, A. P., Walkenhorst, W. F., Westler, W. M., Choe, S., and Markley, J. L. (1993) *Protein Eng. 6*, 221−227.
11. Song, J., Laskowski, M., Jr., Qasim, M. A., and Markley, J. L. (2003) *Biochemistry 42*(10), 2847−2856.
12. Fejzo, J., Westler, W. M., Macura, S., and Markley, J. L. (1991) *J. Magn. Reson. 92*, 195−202.
13. Wang, Y. X., Jacob, J., Cordier, F., Wingfield, P. T., Stahl, S. J., Lee-Huang, S., Torchia, D. A., Grzesiek, S., and Bax, A. (1999) *J. Biomol. NMR 14*, 181−184.
14. Farrow, N. A., Muhandiram, R., Singer, A. U., Pascal, S. M., Kay, C. M., Gish, G., Shoelson, S. E., Pawson, T., Forman-Kay, J. D., and Kay, L. E. (1994) *Biochemistry 33*, 5984−6003.
15. Wishart, D. S., Bigam, C. G., Yao, J., Abildgaard, F., Dyson, H. J., Oldfield, E., Markley, J. L., and Sykes, B. D. (1995) *J. Biomol. NMR 6*, 135−140.
16. Güntert, P., Mumenthaler, C., and Wuthrich, K. (1997) *J. Mol. Biol. 273*, 283−298.
17. Bundi, A., and Wüthrich, K. (1979) *Biopolymers 18*, 299−311.
18. Cornilescu, G., Delaglio, F., and Bax, A. (1999) *J. Biomol. NMR 13*, 289−302.
19. Koradi, R., Billeter, M., and Wüthrich, K. (1996) *J. Mol. Graphics 14*, 51−55.
20. Otting, G., Liepinsh, E., and Wüthrich, K. (1993) *Biochemistry 32*, 3571−3582.
21. Choe, S., Džakula, Z., Kuloglu, E. S., and Markley, J. L. (1998) *J. Biomol. NMR 12*, 193−195.
22. Robertson, A. D., Westler, W. M., and Markley, J. L. (1988) *Biochemistry 27*, 2519−2529.
23. Robertson, A. D., Rhyu, G.-I., Westler, W. M., and Markley, J. L. (1990) *Biopolymers 29*, 461−467.
24. Brandts, J. F., Halvorson, H. R., and Brennan, M. (1975) *Biochemistry 14*, 4953−4963.
25. Kamen, D. E., and Woody, R. W. (2002) *Biochemistry 41*, 4724−4732.
26. Hinck, A. P., Eberhardt, E. S., and Markley, J. L. (1993) *Biochemistry 32*, 11810−11818.
27. Dorman, D. E., Torchia, D. A., and Bovey, F. A. (1973) *Macromolecules 6*, 80−82.
28. Grathwohl, C., and Wüthrich, K. (1976) *Biopolymers 15*, 2025−2041.
29. Schubert, M., Labudde, D., Oschkinat, H., and Schmieder, P. (2002) *J. Biol. NMR 24*, 149−154.
30. Fujinaga, M., Read, R. J., Sielecki, A., Ardelt, W., Laskowski, M., Jr., and James, M. N. (1982) *Proc. Natl. Acad. Sci. U.S.A. 79*, 4868−4872.
31. Fujinaga, M., Sielecki, A. R., Read, R. J., Ardelt, W., Laskowski, M., Jr., and James, M. N. G. (1987) *J. Mol. Biol. 195*, 397−418.

32. Hoogstraten, C. G., Choe, S., Westler, W. M., and Markley, J. L. (1995) *Protein Sci. 4*, 2289−2299.
33. Krezel, A. M., Darba, P., Robertson, A. D., Fejzo, J., Macura, S., and Markley, J. L. (1994) *J. Mol. Biol. 242*, 203-214.
34. Schneider, D. M., Dellwo, M. J., and Wand, A. J. (1992) *Biochemistry 31*, 3645−3652.
35. Grathwohl, C., and Wüthrich, K. (1981) *Biopolymers 20*, 2623−2633.
36. Kim, P. S., and Baldwin, R. L. (1982) *Annu. Rev. Biochem. 51*, 459−489.
37. Richardson, J. S. (1981) *Adv. Protein Chem. 34*, 167−339.
38. Schmid, F. X., and Baldwin, R. L. (1978) *Proc. Natl. Acad. Sci. U.S.A. 75*, 4764−4768.
39. Schmid, F. X., and Baldwin, R. L. (1979) *J. Mol. Biol. 133*, 285−287.
40. Dalessio, P. M., and Ropson, I. J. (2000) *Biochemistry 39*, 860−871.
41. Dyson, H. J., Rance, M., Houghten, R. A., Lerner, R. A., and Wright, P. E. (1988) *J. Mol. Biol. 201*, 161−200.
42. Dyson, H. J., and Wright, P. E. (1998) *Nat. Struct. Biol. 5*, Suppl., 499−503.
43. Galardy, R. E., Bleich, H. E., Ziegler, P., and Craig, L. C. (1976) *Biochemistry 15*, 2303−2309.
44. Kiefhaber, T., Quaas, R., Hahn, U., and Schmid, F. X. (1990) *Biochemistry 29*, 3053−3061.
45. Lin, X., Kaul, S., Rounsley, S., Shea, T. P., Benito, M. I., Town, C. D., Fujii, C. Y., Mason, T., Bowman, C. L., Barnstead, M., Feldblyum, T. V., Buell, C. R., Ketchum, K. A., Lee, J., Ronning, C. M., Koo, H. L., Moffat, K. S., Cronin, L. A., Shen, M., Pai, G., Van Aken, S., Umayam, L., Tallon, L. J., Gill, J. E., and Venter, J. C. (1999) *Nature 402*, 761−768.
46. Skjeldahl, L., Westler, W. M., Oh, B.-H., Krezel, A. M., Holden, H. M., Jacobson, B. L., Rayment, I., and Markley, J. L. (1991) *Biochemistry 30*, 7363−7368.
47. Tollinger, M., Skrynnikov, N. R., Mulder, F. A., Forman-Kay, J. D., and Kay, L. E. (2001) *J. Am. Chem. Soc. 123*, 11341−11352.
48. Read, R. J., Fujinaga, M., Sielecki, A. R., and James, M. N. G. (1983) *Biochemistry 22*, 4420−4433.
49. Clore, G. M., Gronenborn, A. M., James, M. N., Kjaer, M., McPhalen, C. A., and Poulsen, F. M. (1987) *Protein Eng. 1*, 313−318.
50. Eijkelenboom, A. P., Lutzke, R. A., Boelens, R., Plasterk, R. H., Kaptein, R., and Hård, K. (1995) *Nat. Struct. Biol. 2*, 807−810.
51. Holak, T. A., Bode, W., Huber, R., Otlewski, J., and Wilusz, T. (1989) *J. Mol. Biol. 210*, 649−654.
52. Wagner, G., Braun, W., Havel, T. F., Schaumann, T., Go, N., and Wüthrich, K. (1987) *J. Mol. Biol. 196*, 611−639.
53. Wlodawer, A., Nachman, J., Gilliland, G. L., Gallagher, W., and Woodward, C. (1987) *J. Mol. Biol. 198*, 469−480.
54. Yao, J., Dyson, H. J., and Wright, P. E. (1994) *J. Mol. Biol. 243*, 754−766.
55. Yao, J., Feher, V. A., Espejo, B. F., Reymond, M. T., Wright, P. E., and Dyson, H. J. (1994) *J. Mol. Biol. 243*, 736−753.
56. MacArthur, M. W., and Thornton, J. M. (1991) *J. Mol. Biol. 218*, 397−412.
57. Wu, W. J., and Raleigh, D. P. (1998) *Biopolymers 45*, 381−394.
58. Hodel, A., Kautz, R. A., and Fox, R. O. (1995) *Protein Sci. 4*, 484−495.
59. Forsyth, W. R., Gilson, M. K., Antosiewicz, J., Jaren, O. R., and Robertson, A. D. (1998) *Biochemistry 37*, 8643−8652.
60. Forsyth, W. R., and Robertson, A. D. (2000) *Biochemistry 39*, 8067−8072.
61. Garcia-Moreno, B., Dwyer, J. J., Gittis, A. G., Lattman, E. E., Spencer, D. S., and Stites, W. E. (1997) *Biophys. Chem. 64*, 211−224.
62. Honig, B., and Nicholls, A. (1995) *Science 268*, 1144−1149.
63. Ibarra, C., Nieslanik, B. S., and Atkins, W. M. (2001) *Biochemistry 40*, 10614−10624.
64. Matthew, J. B., Gurd, F. R., Garcia-Moreno, B., Flanagan, M. A., March, K. L., and Shire, S. J. (1985) *CRC Crit. Rev. Biochem. 18*, 91−197.
65. Warshel, A., and Russell, S. T. (1984) *Q. Rev. Biophys. 17*, 283−422.
66. March, C. J. (1980) Ph.D. Thesis, Purdue University, West Lafayette, IN.
67. Croll, D. H. (1982) Ph.D. Thesis, Purdue University, West Lafayette, IN.
68. Hemmi, H., Kumazaki, T., Yamazaki, T., Kojima, S., Yoshida, T., Kyogoku, Y., Katsu, M., Shinohara, F., Yokosawa, H., Miura, K., and Kobayashi, Y. (2003) *Biochemistry 42*, 2524−2534.
69. Hemmi, H., Yoshida, T., Kumazaki, T., Nemoto, N., Hasegawa, J., Nishioka, F., Kyogoku, Y., Yokosawa, H., and Kobayashi, Y. (2002) *Biochemistry 41*, 10657−10664.

BI034053F